Core collapse supernovae in the QCD phase diagram

T. Fischer,[1,2,*] D. Blaschke,[3,4] M. Hempel,[5] T. Klähn,[3]
R. Łastowiecki,[3] M. Liebendörfer,[5] G. Martínez-Pinedo,[1,2] G. Pagliara,[6]
I. Sagert,[6] F. Sandin,[7,8] J. Schaffner-Bielich,[6] and S. Typel[1,9]

[1] *GSI, Helmholtzzentrum für Schwerionenforschung GmbH, Darmstadt, Germany*

[2] *Technische Universität Darmstadt, Germany*

[3] *Institute for Theoretical Physics, University of Wroclaw, Poland*

[4] *Bogoliubov Laboratory of Theoretical Physics, JINR Dubna, Russia*

[5] *Department of Physics, University of Basel, Switzerland*

[6] *Institut für Theoretische Physik, Ruprecht-Karls-Universität, Heidelberg, Germany*

[7] *Department of Computer Science and Electrical Engineering,*
EISLAB, Luleå Tekniska Universitet, Luleå, Sweden

[8] *Département AGO-IFPA, Université Liege, Belgium*

[9] *Excellence Cluster Universe, Technische Universität München, Germany*

We compare two classes of hybrid equations of state with a hadron-to-quark matter phase transition in their application to core collapse supernova simulations. The first one uses the quark bag model and describes the transition to three-flavor quark matter at low critical densities. The second one employs a Polyakov-loop extended Nambu–Jona–Lasinio (PNJL) model with parameters describing a phase transition to two-flavor quark matter at higher critical densities. These models possess a distinctly different temperature dependence of their transition densities which turns out to be crucial for the possible appearance of quark matter in supernova cores. During the early post bounce accretion phase quark matter is found only if the phase transition takes place at sufficiently low densities as in the study based on the bag model. The increase critical density with increasing temperature, as obtained for our PNJL parametrization, prevents the formation of quark matter. The further evolution of the core collapse supernova as obtained applying the quark bag model leads to a structural reconfiguration of the central protoneutron star where, in addition to a massive pure quark matter core, a strong hydrodynamic shock wave forms and a second neutrino burst is released during the shock propagation across the neu-

trinospheres. We discuss the severe constraints in the freedom of choice of quark matter models and their parametrization due to the recently observed 2 $M_\odot$ pulsar and their implications for further studies of core collapse supernovae in the QCD phase diagram.

1. INTRODUCTION

Stars more massive than 8 $M_\odot$ explode as core collapse supernovae, with kinetic explosion energies of the ejected material on the order of 10^{51} erg. The remnants, the protoneutron stars (PNSs), are initially hot and lepton-rich and cool via deleptonization during the first 30 seconds after the onset of the explosion. Above a certain progenitor mass threshold on the order of 40 $M_\odot$, which is an active subject of research, stars will no longer explode. Such models will collapse and from black holes. The critical mass for a PNS to collapse and from a black hole is given by the equation of state (EoS). The commonly used EoS in core collapse supernova simulations are based on pure hadronic descriptions, e.g. the compressible liquid-drop model with surface effects [1] and relativistic mean field theory including the Thomas-Fermi approximation for heavy nuclei [2]. The conditions that are obtained in PNS interiors during the simulation, are several times nuclear matter density, temperatures on the order of several tens of MeV and a low proton-to-baryon ratio given by the electron fraction of[1] $Y_e = Y_p \leq 0.3$. Under such conditions, the quark-hadron phase transition is not unlikely to take place and the assumption of pure hadronic matter becomes questionable. Ab initio calculations of the phase diagram and EoS of quantum chromodynamics (QCD) as the fundamental theory of strongly interacting matter come from simulations of this gauge theory on the lattice but are still restricted to low baryon densities (chemical potentials). In this region of the phase diagram they predict a crossover transition with a pseudocritical temperature for chiral symmetry restoration and deconfinement at $T_c \simeq 150 - 170$ MeV [3, 4]. A critical endpoint for first order transitions is conjectured but lies, if it exists at all, outside the region presently accessible by lattice QCD. An interesting conjecture supported

* Electronic address: t.fischer@gsi.de

[1] The proton-to-baryon ratio, $Y_p = n_p/n_B$, is equal to the electron fraction, $Y_e := Y_{e^-} - Y_{e^+}$, in the absence of muons.

by a statistical model analysis of hadron production in heavy-ion collisions and by the large-N_c limit of QCD suggests the existence of a triple point in the phase diagram [5] due to a third, "quarkyonic" phase at temperatures $T < T_c$ and high baryon densities [6]. This state of matter might become accessible in experiments at the planned third generation of heavy-ion collision facilities FAIR in Darmstadt (Germany) and NICA in Dubna (Russia) [7] which thus allow systematic laboratory studies of conditions like in supernova collapse and protoneutron star evolution [8].

In order to investigate the appearance of quark matter in core collapse supernova models, the implementation of a quark-hadron hybrid EoS is required. It must be valid for a large range of densities n_B, temperatures T and proton-to-baryon ratios. At large baryon densities, where lattice QCD cannot be applied due to current conceptional limitations, phenomenological models are commonly used. In the present study we will discuss hybrid EoS which employ quark matter models that are representative examples from two wide classes: bag models and NJL-type models. The popular and simple thermodynamical bag model is inspired by the success of the vacuum MIT bag model for the hadron spectrum [9]. It describes quarks as non-interacting fermions of a constant mass confined by an external "bag" pressure B. NJL-type models are constructed to obey basic symmetries of the QCD Lagrangian like the chiral symmetry of light quarks, and to describe its dynamical breaking which results in medium-dependent masses (see [10] and references therein). The inclusion of diquark interaction channels leads to a rich phase structure at low temperatures and high densities with color superconductivity (diquark condensation) in two-flavor (2SC) and three-flavor (CFL) quark matter (see, e.g., [11] for the phase structure and [12] for the relevance to protoneutron stars; detailed information concerning color superconductivity is found in review articles [10, 13]). These models have no confining interaction and would therefore lead to the unphysical dominance of thermal quark excitations already at temperatures well below T_c. Their coupling to the Polyakov loop potential is essential to suppress the unphysical degrees of freedom and it can be adjusted to fit the behavior of lattice QCD thermodynamics at low densities [14]. Extending this effective model to high densities leads to the class of PNJL models of which we apply one for this study.

Different assumptions made for the description of quark matter lead to different critical conditions for the onset of deconfinement, which are given in terms of a critical density that depends on the temperature and the proton-to-baryon ratio. The resulting different phase

diagrams may lead to a different evolutionary behavior for core collapse supernovae. The central supernova conditions start from low densities (6×10^{-6} fm^{-3}/10^{10} g cm^{-3}) and temperatures (0.6 MeV), where pure hadronic matter dominates, and approach densities above nuclear saturation density (0.16 fm^{-1}/2.7×10^{14} g cm^{-3}) at temperatures on the order to tens of MeV and $Y_p \simeq 0.2 - 0.3$. The nature of the QCD transition is not precisely understood on a microscopic level. Therefore, one usually splices independent nuclear and quark matter EoS by constructing the phase transition using more or less appropriate conditions for the phase equilibrium. Popular examples are the Maxwell, Gibbs or Glendenning [15] constructions, whereby usually the Maxwell construction leads to the smallest region between critical densities for the onset and the end of the mixed phase. We will disregard finite size effects (pasta structures) and also non-equilibrium effects due to the nucleation of the new phase with the justification that weak processes establishing the chemical equilibrium are fast compared to the typical timescales encountered in supernova simulations [16]. We will compare the evolution of a representative core collapse supernova simulation in the two different phase diagrams based on the bag model and the PNJL model. The core collapse supernova model is based on general relativistic radiation hydrodynamics and three flavor Boltzmann neutrino transport [17–22]

The manuscript is organized as follows: In Sect. 2 we introduce the standard core collapse supernova phenomenology. In Sect. 3 we briefly introduce the two quark-hadron hybrid EoS, the quark bag model and the PNJL model. The evolution of a representative 15 $M_\odot$ core collapse supernova model in the phase diagram is illustrated in Sect. 4 by comparing the quark bag and PNJL models. We close with a summary in Sect. 5.

2. THE STANDARD SCENARIO OF CORE COLLAPSE SUPERNOVAE

Si-burning produces Fe-cores at the final phase of stellar evolution of massive stars. These Fe-cores start to contract due to the photodisintegration of heavy elements and electron captures. The latter reduces the dominant pressure of the degenerate electron gas. During the collapse, density and temperature rise and hence electron captures, which deleptonize the central core, increase. The collapse accelerates until neutrino trapping densities, on the order of $\rho \simeq 10^{11}$–10^{13} g/cm^3, are obtained after which the collapse proceeds adiabatically. At nuclear matter density, the repulsive nuclear interaction stiffens the EoS significantly and

the collapse halts. The core bounces back, where a sound wave forms, which steepens into a shock wave. The shock wave propagates outwards where the dissociation of infalling heavy nuclei causes an energy loss of about 8 MeV per baryon. Furthermore, during the shock propagation across the neutrinospheres, which are the neutrino energy and flavor dependent spheres of last scattering, additional electron captures release a burst of ν_e that carries away 4–5 $\times 10^{53}$ erg/s on a short timescale of 5–20 ms post bounce (depending on the progenitor model and the EoS). Both sources of energy loss turn the dynamic shock into a standing accretion shock, already at about 5 ms post bounce.

The post bounce evolution is determined by mass accretion, due to the continuously infalling material from the outer layers of the Fe-core as well as the surrounding Si-layer (depending on the progenitor model). On a timescale on the order of 100 ms up to seconds, the central density and temperature increase continuously. In order to achieve an explosion, energy needs to be deposit behind the standing accretion shock which subsequently revives the standing accretion shock. Several mechanisms have been suggested, including the magnetically-driven [23–25], the acoustic [26] and the neutrino-driven [27]. The standard scenario, delayed explosions due to neutrino heating, have been shown to work in spherical symmetry [28, 29] for the low mass 8.8 $M_\odot$ ONeMg-core [30–32]. For more massive progenitors, multi-dimensional phenomena such as rotation and the development of fluid instabilities are required and help to increase the neutrino heating efficiency [33–36]. Such models are also required to aid the understanding of aspherical explosions [37, 38].

3. THE QUARK BAG AND PNJL HYBRID MODELS

We discuss two different quark matter descriptions for use in astrophysical applications as well as their differences in the resulting EoS. The quark bag model for three flavor quark matter is described in detail in the Refs. [39–41]. Bag constants in the range of $B^{1/4}$ =155–165 MeV and corrections from the strong interaction were adopted and a fixed strange quark mass of 100 MeV is applied in these simulations which we want to contrast here with first results for a PNJL model. A serious drawback of the bag model parametrization employed here is that cannot describe the mass of the recently observed 1.97 $M_\odot$ neutron star [42]. This could be cured by extending the bag model and accounting for leading order QCD corrections and diquark condensation [43, 44] but results in an early onset of quark matter

only for considerably stiff nuclear EoS.

The three flavor quark matter PNJL model is based on the description in Ref. [11, 12] with the Polyakov loop extension according to [14]. An additional isoscalar vector meson interaction leads to a stiffening of the quark matter equation of state and allows to describe hybrid stars with a mass of 2 $M_\odot$ [45]. The diquark and vector meson coupling is set to $\eta_D = 1.02$ and $\eta_V = 0.25$, respectively. Strangeness on the quark side in the PNJL model occurs at higher densities than the onset of deconfinement, due to the dynamical quark masses involved. The resulting phase diagram is discussed in Ref. [7].

The Figs. 1(a) and 1(b) compare the phase diagrams for the quark bag model and the PNJL model for different proton-to-baryon ratios Y_p relevant for supernova matter. There are different critical densities for the onset of deconfinement comparing the quark bag and PNJL models for equal Y_p. E.g. for $Y_p = 0.3$ and $T = 0$, the critical densities are 0.159 fm^{-1} for the bag model in comparison to 0.214 fm^{-1} for the PNJL model (see the solid lines in the Figs. 1(a) and 1(b)). For the bag model, the early onset of deconfinement close to normal nuclear matter density illustrates the strong isospin dependency of the critical density. For instance, at higher $Y_p = 0.5$ the critical density shifts to 0.321 fm^{-1} for $T = 0$. In general, small transition densities result from the application of the Gibbs conditions for the phase transition with the corresponding extended mixed phase and from the existence of the s-quark flavor which results in a larger number of degrees of freedom when compared to nuclear matter. For the PNJL model, the transition to quark matter, shown in Fig. 1(b), is based on the Maxwell construction. The critical densities are generally larger and the mixed phase is very narrow in density compared to the quark bag model. The PNJL model also shows the typical isospin dependency. The critical density reduces at decreasing Y_p, which is however much weaker than for the quark bag model. Both models differ also significantly in the maximum mass of neutron stars, 1.50 $M_\odot$ for the bag model with $B^{1/4} = 165$ MeV and 1.97 $M_\odot$ for the PNJL model.

Furthermore, the temperature dependence of the critical density is different in both quark matter descriptions. This is of particular relevance for astrophysical applications that explore a possible quark-hadron phase transition. In the quark bag model, the critical density reduces continuously at higher temperatures. It reaches about 0.1 fm^{-1} at $T = 50$ MeV for $Y_p = 0.3$. For the PNJL model, the critical density rises with increasing temperature for any Y_p. This behavior is a result of the neglect of any modification of the Polyakov loop potential on the

quark density and should be improved as soon as reasonable constraints for such a procedure can be defined, see [46] for a first step.

The resulting EoS are illustrated in Figs. 2(a) and 2(b), showing the pressure-density curves for different entropies per baryon and fixed $Y_p = 0.3$. The largely extended mixed phase region in the phase diagram for the bag model corresponds to a soft EoS. This is illustrated via the pressure-density curves in Fig. 2(a), where the adiabatic index differs initially only little between the onset of deconfinement and the pure hadronic phase. Towards the end of the mixed phase where the pure quark phase sets in, the adiabatic index is largely reduced for any entropy per baryon and hence the EoS is significantly softer compared to the hadronic case. In the pure quark phase, the adiabatic index increases again significantly, which makes the pure quark phase stiffer than the mixed phase. The sharp transition between the mixed and the pure quark phases, gives rise to a strong effect for the hydrodynamics evolution along isentropes.

The PNJL hybrid EoS shows a different pressure behavior (see Fig. 2(b)) during the quark-hadron phase transition. The largest change of the adiabatic index is found at the onset of deconfinement. Close to the onset of pure quark matter, the adiabatic index changes only little. These two aspects are a general feature of the chosen construction of the PNJL hybrid EoS, for which a smooth transition can be expected in dynamical simulations.

4. CORE COLLAPSE SUPERNOVA EVOLUTION IN THE PHASE DIAGRAM

The central temperature and density evolution of the 15 $M_\odot$ core collapse supernova simulation is shown via the dashed lines in the Figs. 1(a) and 1(b), for the first second post bounce, during which the explosion is expected to take place for such massive Fe-core progenitors [38]. This phase of the supernova is determined by mass accretion (~ 0.1 $M_\odot$/s) onto the central PNS, which consequently contracts on a timescale between 100 ms up to seconds. During the PNS contraction, the central density and temperature rise continuously[2]. During this evolution, the central electron fraction reduced from $Y_p \simeq 0.3$ to $Y_p \simeq 0.25$. The simulation is based on a pure hadronic description of matter [2]. The current supernova models explore only hadronic EoS. It is shown here to illustrate the possibility and the

[2] The highest temperatures $\sim 30 - 60$ MeV are not obtained at the center of the PNS but at slightly lower densities; it corresponds to the region where the bounce shock formed initially.

conditions relevant in order to obtain quark matter at supernova cores.

The differences between the two hybrid EoS become clear. Using the quark bag model, it is possible to obtain quark matter. The early post bounce evolution of the central mass trajectories considered for the 15 $M_\odot$ progenitor model, enter deeply into the mixed phase. The same holds true for the non-central part of the PNS, where up to 0.5 $M_\odot$ can reach the mixed phase within the first 500 ms post bounce evolution (depending on the progenitor model [41]). Within the PNJL model, the central densities obtained for this particular 15 $M_\odot$ core collapse supernova simulation are not sufficiently high enough to enter the mixed phase. It would require an additional rise of the central density by a factor of two or more. For such quark-hadron hybrid EoS quark matter will not be reached in core collapse supernovae of massive stars up to 15 $M_\odot$ as discussed here, during the expected explosion phase of 0.5–1 seconds post bounce.

In order to investigate the EoS softening effects from the presence of quark matter in the PNS interior and possible consequences for the dynamical evolution (and possible observations), we apply the quark bag model hybrid EoS (using $B^{1/4} = 155$ MeV, $\alpha_S = 0.3$) to a core collapse supernova evolution (again the 15 $M_\odot$ model). The largely reduced adiabatic index at the end of the mixed phase causes a gravitational collapse of the PNS, spatially separated into central sub-sonic collapse and outer super-sonic collapse. During the collapse density and temperature rise (see Fig. 3), which in turn favors pure quark matter over hadronic matter. In the pure quark phase, where the adiabatic index is increased, the collapse halts and a strong hydrodynamic shock front forms. This was first observed in the context of a first order deconfinement phase transition in ref. [48], in relation to the statistically insignificant multi-peaked neutrino signal form SN1987A [49], and later discussed in more detail in the refs. [50, 51]. The shock wave appears initially as a pure accretion front, which is illustrated in Fig. 3 at 310.4668 ms post bounce. The shock propagates outwards in radius towards the PNS surface, driven by the thermal pressure of the deconfined quarks and neutrino heating behind the shock. The latter aspect is related to local heating rates due to electron (anti)neutrino absorptions, which increase at the quark-hadron phase boundary where the infalling hadronic material converts into quark matter and density and temperature rise by several orders of magnitude. At the PNS surface, where the density decreases over several orders of magnitude, the accretion front accelerates and positive velocities are obtained (see Fig. 3 at 310.5135 ms post bounce). This moment determines the onset of explosion, even

in core collapse supernova models where otherwise (i.e. without the quark-hadron phase transition) no explosions could have been obtained. The shock expands and continues to accelerate where matter velocities on the order of 10^5 km/s are obtained.

The shock propagation across the neutrinospheres releases an additional burst of neutrinos, illustrated in Fig. 4. This second burst rises in all neutrino flavors. It differs from the reference case discussed in ref. [41], where the second burst was dominated by $\bar{\nu}_e$ and ($\nu_{\mu/\tau}$, $\bar{\nu}_{\mu/\tau}$) due to the lower density of the PNS envelope of the less massive progenitor chosen and the different quark bag EoS parameters. The rise of the burst is due to the presence of numerous electron-positron pairs that allow for the production of ν_e and $\bar{\nu}_e$ via the charged current reactions as well as ($\nu_{\mu/\tau}$, $\bar{\nu}_{\mu/\tau}$) via pair processes. It differs from the deleptonization burst at core bounce, which is only in ν_e emitted via a large number of electron captures. This second burst, if occurring, is a strong observational indication for the reconfiguration of the high density domain in core collapse supernova evolution.

Coming back to the PNJL model in core collapse supernova simulations, preliminary results of long-term non-exploding models in the progenitor mass range between 15–25 $M_\odot$, show a smooth transition to quark matter at the PNS interior where only the mixed phase could be reached. Very little mass (~ 0.05 $M_\odot$) is converted into the mixed phase and the quark fraction rises only on timescales on the order of seconds, which corresponds to the PNS contraction timescale induced via mass accretion. However, massive star explosions are expected to take place during the first 0.5–1 seconds post bounce. Hence, a direct correlation to the explosion mechanism of massive stars as well as direct observables that relate to the explosion phase, cannot be expected for such a hybrid EoS. However, this hybrid EoS model has another interesting feature. Since the PNJL model possesses a critical point, one may study whether in the collapse of very massive progenitors with subsequent black hole formation the trajectory of the collapse in the QCD phase diagram sweeps the critical point before horizon crossing [52]. In that case a characteristic modification of possible observables from the deconfinement transition is expected, at variance to trajectories which do not pass the critical point. The realistic modeling of such processes requires further development of a phase transition construction which does not remove the critical endpoint.

5. SUMMARY

We discussed the possibility to reach the critical conditions for the onset of deconfinement in core collapse supernovae, comparing two different quark-hadron hybrid EoS. Based on the bag model for strange quark matter and choices of low bag constants, without violating constraints from e.g. heavy-ion collision experiments, the low critical densities as well as the strong isospin and temperature dependencies allow for the quark-hadron phase transition to take place in core collapse supernova simulations within the first 500 ms post bounce. For a particular choice of parameters, we illustrated the dynamical evolution. It was determined by an adiabatic collapse due to the soft EoS in the extended mixed phase modeled by applying Gibbs conditions, and the formation of a strong hydrodynamic shock wave. It triggered the explosion even in models where otherwise explosions could not be obtained. Furthermore, the millisecond neutrino burst released from the shock propagation across the neutrinospheres may become observable for a future Galactic event if quark matter occurs [53]. The future observation of such a multi-peaked neutrino signal may reveal information about the nuclear EoS at high densities and temperatures that cannot be reached in heavy-ion collision experiments at present. For the PNJL model parametrization presented here, the higher critical density and the narrow mixed phase due to the Maxwell construction, together with the rising critical density for increasing temperatures, prevent the quark-hadron phase transition to occur in core collapse supernova simulations during the post bounce accretion phase. For such an EoS, a direct correlation between the phase transition to quark matter and the explosion mechanism cannot be expected. However, the conditions for the appearance of quark matter for the PNJL model may allow to obtain a signal from core collapse supernovae during the PNS deleptonization phase, on timescales on the order of several seconds after the onset of, e.g., initially neutrino-driven explosions.

The two classes of hybrid EoS discussed here allow for very different types of investigations in simulations of core collapse supernovae. Hybrid EoS based on the class of bag models for quark matter give access to bulk properties of quark-hadron matter and allow to model EoS which undergo a quark-hadron phase transition during the supernova collapse accompanied by a second neutrino burst. However, the bag model cannot capture the aspect of chiral symmetry restoration and possible effects of the existence of a critical point. Moreover, it remains to be shown whether the 2 $M_\odot$ mass constraint can be explained in agreement

with the deconfinement scenario for this class of models. The hybrid models based on a PNJL-type approach to quark matter would allow to study the question of the existence of critical points in the QCD phase diagram, e.g., during black hole formation where high temperatures on the order of several 100 MeV are obtained. A systematic study of possible observables from black hole formation using PNJL models that include a critical endpoint, may provide the astrophysical analogue of the energy scan programs in heavy-ion collisions. However, the 2 $M_\odot$ mass constraint is obtained at the price of a too high critical density for a deconfinement transition during collapse. This statement is not the final word. It is possible, e.g., via a density dependence of the gluon thermodynamics which is absent in the present model, to allow for a simultaneous description of deconfinement in the supernova interior and high mass (proto) neutron stars.

ACKNOWLEDGMENT

The authors would like to thank Hovik Grigorian for his comments and helpful discussions. The project was funded by the Swiss National Science Foundation (SNF) under project numbers PP00P2-124879/1, 200020-122287, and the Helmholtz Research School for Quark Matter Studies. T.F. is supported the SNF under project number PBBSP2-133378 and by HIC for FAIR. G.M.P. is partly supported by the Sonderforschungsbereich 634, the ExtreMe Matter Institute EMMI, the Helmholtz International Center for FAIR, and the Helmholtz Association through the Nuclear Astrophysics Virtual Institute (VH-VI-417). D.B., T.K. and R.Ł. receive support from the Polish Ministry for Science and Higher Education. D.B. acknowledges support from the Russian Fund for Basic Research under grant No. 11-02-01538-a. R. Ł. received support from the Bogoliubov-Infeld programme for visiting JINR at Dubna where part of his work was done. The work of G.P. is supported by the Deutsche Forschungsgemeinschaft (DFG) under Grant No. PA 1780/2-1 and J.S.-B. is supported by the DFG through the Heidelberg Graduate School of Fundamental Physics. M.H. acknowledges support from the High Performance and High Productivity Computing (HP2C) project. S.T. is supported by the DFG cluster of excellence "Origin and Structure of the Universe". F.S. acknowledges support from the Belgian fund for scientific research (FNRS). I.S. is supported by the Alexander von Humboldt foundation via a Feodor Lynen fellowship and wishes to acknowledge the support of the Michigan State University High

Performance Computing Center and the Institute for Cyber Enabled Research. The authors are additionally supported by CompStar, a research networking program of the European Science Foundation, and the Scopes project funded by the Swiss National Science Foundation grant. no. IB7320-110996/1.

---

1. J. M. Lattimer and F. D. Swesty, Nucl. Phys. A **535**, 331 (1991).
2. H. Shen, H. Toki, K. Oyamatsu and K. Sumiyoshi, Prog. Theor. Phys. **100**, 1013 (1998).
3. S. Borsanyi, Z. Fodor, C. Hoelbling, S. D. Katz, S. Krieg, C. Ratti and K. K. Szabo [Wuppertal-Budapest Collaboration], JHEP **1009**, 073 (2010).
4. A. Bazavov and P. Petreczky [HotQCD Collaboration], arXiv:1009.4914 [hep-lat].
5. A. Andronic *et al.*, Nucl. Phys. A **837**, 65 (2010).
6. L. McLerran and R. D. Pisarski, Nucl. Phys. A **796**, 83 (2007).
7. D. B. Blaschke, F. Sandin, V. V. Skokov and S. Typel, Acta Phys. Polon. Supp. **3**, 741 (2010).
8. T. Klähn, D. Blaschke and F. Weber, arXiv:1101.6061 [nucl-th].
9. C. E. DeTar and J. F. Donoghue, Ann. Rev. Nucl. Part. Sci. **33**, 235 (1983).
10. M. Buballa, Phys. Rept. **407**, 205 (2005).
11. D. Blaschke, S. Fredriksson, H. Grigorian, A. M. Öztas and F. Sandin, Phys. Rev. D **72**, 065020 (2005).
12. F. Sandin and D. Blaschke, Phys. Rev. D **75**, 125013 (2007).
13. M. G. Alford, A. Schmitt, K. Rajagopal and T. Schafer, Rev. Mod. Phys. **80**, 1455 (2008).
14. S. Roessner, C. Ratti and W. Weise, Phys. Rev. D **75**, 034007 (2007).
15. N. K. Glendenning, Phys. Rev. D **46**, 1274 (1992).
16. B. W. Mintz, E. S. Fraga, G. Pagliara and J. Schaffner-Bielich, Phys. Rev. D **81**, 123012 (2010).
17. A. Mezzacappa and S. W. Bruenn, Astrophys. J. **405**, 637 (1993).
18. A. Mezzacappa and S. W. Bruenn, Astrophys. J. **405**, 669 (1993).
19. A. Mezzacappa and S. W. Bruenn, Astrophys. J. **410**, 740 (1993).
20. M. Liebendoerfer, A. Mezzacappa, F. K. Thielemann, O. E. B. Messer, W. R. Hix and S. W. Bruenn, Phys. Rev. D **63**, 103004 (2001).
21. M. Liebendoerfer, A. Mezzacappa and F. K. Thielemann, Phys. Rev. D **63**, 104003 (2001).
22. M. Liebendoerfer, O. E. B. Messer, A. Mezzacappa, S. W. Bruenn, C. Y. Cardall and

F. K. Thielemann, Astrophys. J. Suppl. **150**, 263 (2004).

23. J. M. LeBlanc and J. R. Wilson, Astrophys. J. **161**, 541 (1970).
24. S. G. Moiseenko and G. S. Bisnovatyi-Kogan, Astrophys. Space Sci. **311**, 191 (2007).
25. T. Takiwaki, K. Kotake and K. Sato, Astrophys. J. **691**, 1360 (2009).
26. A. Burrows, E. Livne, L. Dessart, C. Ott and J. Murphy, New Astron. Rev. **50**, 487 (2006).
27. H. A. Bethe and J. R. Wilson, Astrophys. J. **295**, 14 (1985).
28. F. S. Kitaura, H. T. Janka and W. Hillebrandt, Astrophys. J. **450**, 345 (2006).
29. T. Fischer, S. C. Whitehouse, A. Mezzacappa, F. K. Thielemann and M. Liebendorfer, Astron. Astrophys. **517**, A80 (2010).
30. K. Nomoto, in *Supernova Remnants and their X-ray Emission*, Eds. J. Danziger and P. Gorenstein, IAU Symposium **101**, p. 139 (1983).
31. K. Nomoto, Astrophys. J. **277**, 791 (1984).
32. K. Nomoto, Astrophys. J. **322**, 206 (1987).
33. D. S. Miller, J. R. Wilson and R. W. Mayle, Astrophys. J. **415**, 278 (1993).
34. M. Herant, W. Benz, W. R. Hix, C. L. Fryer and S. A. Colgate, Astrophys. J. **435**, 339 (1994).
35. A. Burrows, J. Hayes and B. A. Fryxell, Astrophys. J. **450**, 830 (1995).
36. H.-T. Janka and E. Mueller, Astron. Astrophys. **306**, 167 (1996).
37. S. W. Bruenn, A. Mezzacappa, W. R. Hix, J. M. Blondin, P. Marronetti, O. E. B. Messer, C. J. Dirk and S. Joshida, J. Phys. Conf. Ser. **180**, 012018 (2009).
38. A. Marek and H.-Th. Janka, Astrophys. J. **694**, 664 (2009).
39. I. Sagert *et al.*, Phys. Rev. Lett. **102**, 081101 (2009).
40. T. Fischer, I. Sagert, M. Hempel, G. Pagliara, J. Schaffner-Bielich and M. Liebendörfer, Class. Quant. Grav. **27**, 114102 (2010).
41. T. Fischer *et al.*, arXiv:1011.3409 [astro-ph.HE].
42. P. Demorest, T. Pennucci, S. Ransom, M. Roberts and J. Hessels, Nature **467**, 1081 (2010).
43. F. Özel, D. Psaltis, S. Ransom, P. Demorest and M. Alford, Astrophys. J. **724**, L199 (2010).
44. S. Weissenborn, I. Sagert, G. Pagliara, M. Hempel and J. Schaffner-Bielich, arXiv:1102.2869 [astro-ph.HE].
45. T. Klähn *et al.*, Phys. Lett. B **654**, 170 (2007).
46. D. Blaschke, J. Berdermann and R. Łastowiecki, Prog. Theor. Phys. Suppl. **186**, 81 (2010).
47. S. E. Woosley, A. Heger and T. A. Weaver, Rev. Mod. Phys. **74**, 1015 (2002).

48. T. Takahara and K. Sato, Astrophys. J. **335**, 301 (1988).

49. K. S. Hirata et al., Phys. Rev. D **38**, 448 (1988).

50. N. A. Gentile, M. B. Aufderheide, G. J. Mathews, F. D. Swesty and G. M. Fuller, Astrophys. J. **414**, 701 (1993).

51. H. Grigorian, B. Hermann and F. Weber, Physics of Particles and Nuclei **30**, 156 (1999).

52. A. Ohnishi, H. Ueda, T. Z. Nakano, M. Ruggieri and K. Sumiyoshi, arXiv:1102.3753 [nucl-th].

53. B. Dasgupta, T. Fischer, S. Horiuchi, M. Liebendörfer, A. Mirizzi, I. Sagert and J. Schaffner-Bielich, Phys. Rev. D **81**, 103005 (2010).

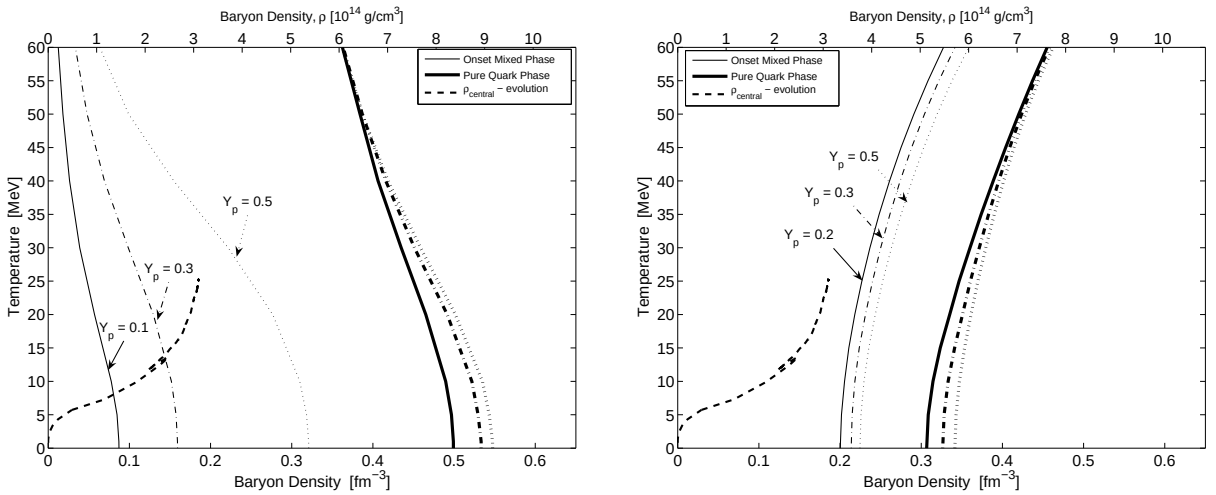

(a) Quark bag model ($B^{1/4} = 165$ MeV), for $Y_p = 0.1$ (solid lines), $Y_p = 0.3$ (dash-dotted lines) and $Y_p = 0.5$ (dotted lines)

(b) PNJL model ($\eta_D = 1.02$, $\eta_V = 0.25$), for $Y_p = 0.2$ (solid lines), $Y_p = 0.3$ (dash-dotted lines) and $Y_p = 0.5$ (dotted lines)

Figure 1. QCD phase diagrams for the two hybrid EoS under discussion (onset of quark matter: thin lines, pure quark phase: thick lines) for selected proton-to-baryon ratios Y_p that are indicated via the text arrows in the graphs. The dashed line shows the evolution of the central temperature and density for a representative core collapse supernova of a 15 $M_\odot$ progenitor model [47], based on a hadronic EoS [2] for the first second post bounce. Note the kink between 0.12–0.15 fm^{-1}, it is related to the core bounce after which the central density and temperature decrease slightly before they continue to increase during the later compression. The wide stretched mixed phase region for the bag model in graph (a) results from the applied Gibbs construction while the in comparison narrow region for the PNJL model in graph (b) is a result of the Maxwell construction.

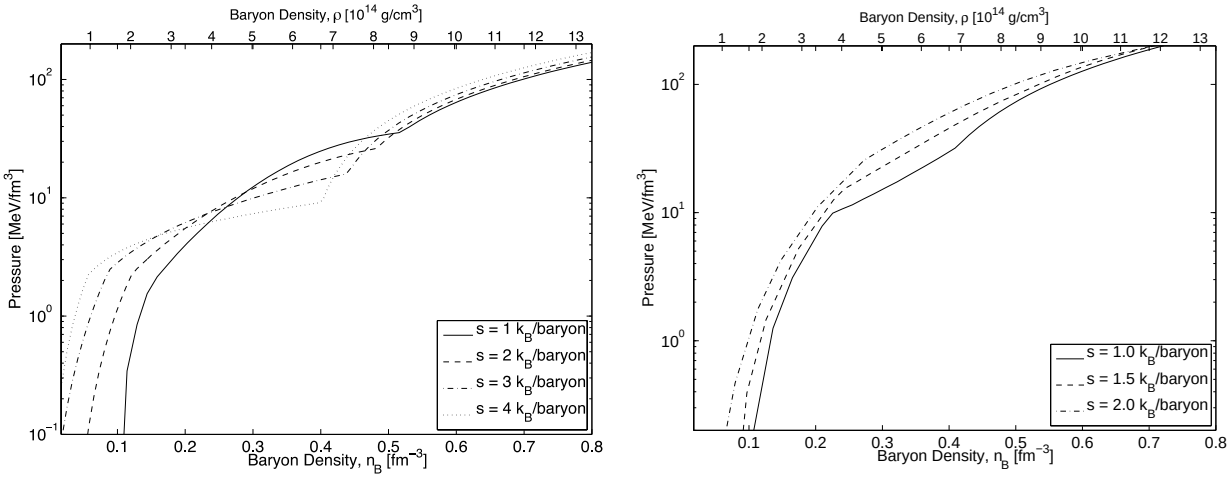

(a) Quark bag model ($B^{1/4} = 165$ MeV). (b) PNJL model ($\eta_D = 1.02$, $\eta_V = 0.25$).

Figure 2. Total pressure density curves for different entropies per baryon and fixed $Y_p = 0.3$, based on the two hybrid EoS.

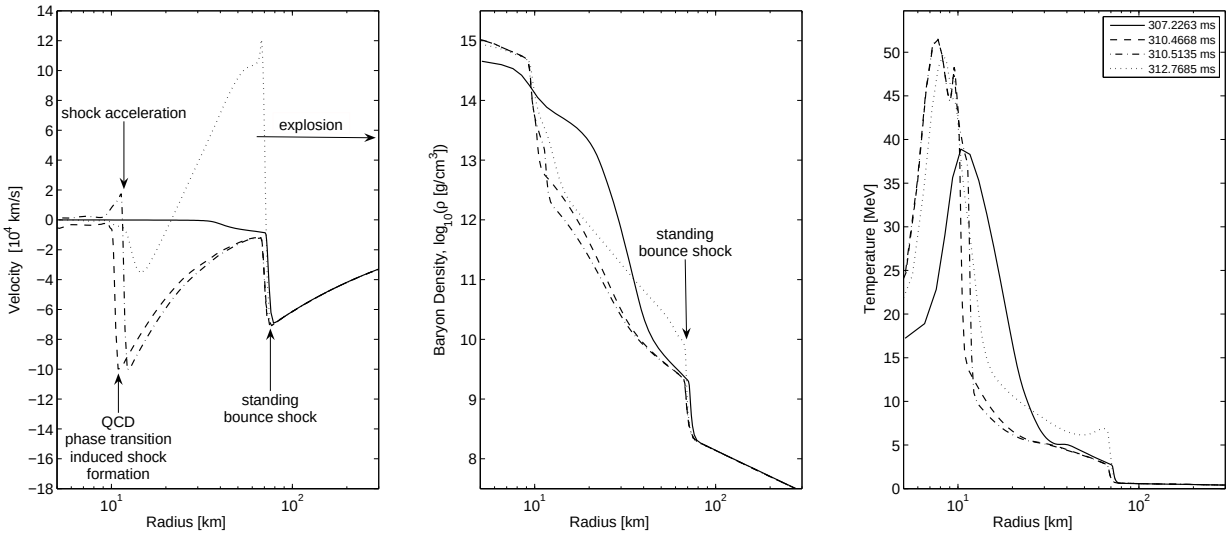

Figure 3. Radial profiles of velocity, density and temperature for a 15 $M_\odot$ progenitor model at selected post bounce times during the QCD phase transition induced PNS collapse, using the bag model with $B^{1/4} = 155$ MeV and $\alpha_S = 0.3$.

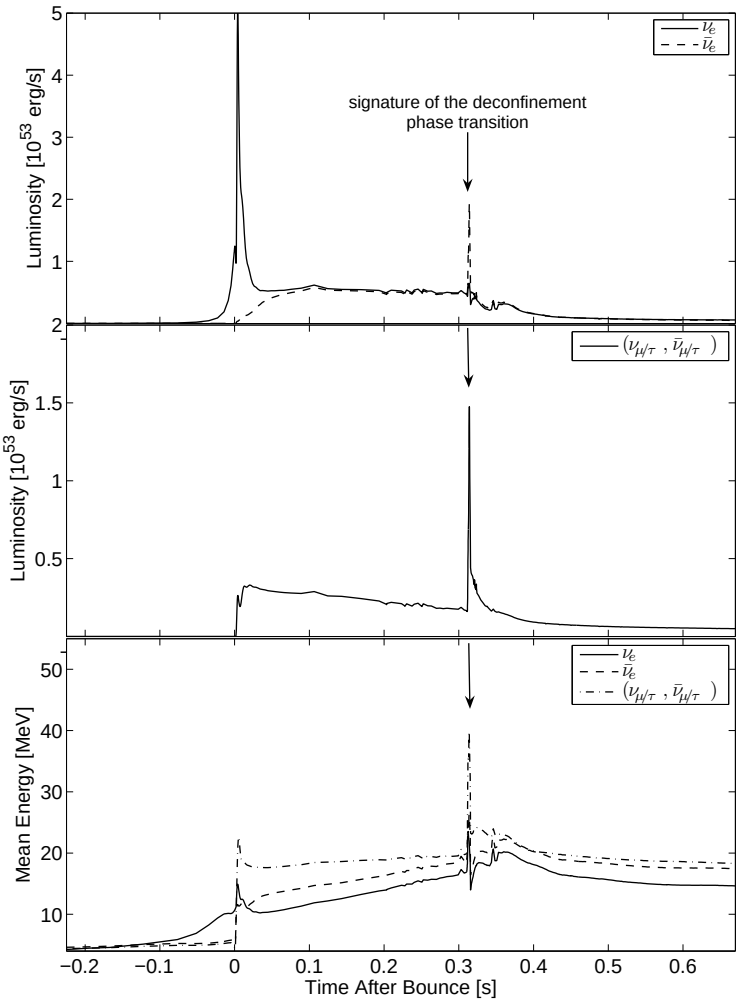

Figure 4. Evolution of the neutrino luminosities and mean energies for a 15 $M_\odot$ model, including the quark hadron phase transition using the quark bag model ($B^{1/4} = 155$ MeV, $\alpha_S = 0.3$) [40, 41]. Due to the phase transition, the PNS becomes gravitational unstable and collapses. The critical conditions for the gravitational collapse ($T = 17.67$ MeV, $\rho = 5.511 \times 10^{14}$ g/cm^3, $Y_p = 0.197$) are obtained at about 308 ms after bounce for this particular model. The second burst is released when the second shock, that forms due to the quark hadron phase transition in the PNS interior, crosses the neutrinospheres. The second burst occurs in all neutrino flavors, while the deleptonization burst at core bounce appears only in ν_e. This signature of deconfinement is absent in models that explore standard hadronic EoSs (e.g. from ref. [2]).

FIGURE CAPTIONS

1. QCD phase diagrams for the two hybrid EoS under discussion (onset of quark matter: thin lines, pure quark phase: thick lines) for selected proton-to-baryon ratios Y_p that are indicated via the text arrows in the graphs. The dashed line shows the evolution of the central temperature and density for a representative core collapse supernova of a 15 $M_\odot$ progenitor model [47], based on a hadronic EoS [2] for the first second post bounce. Note the kink between 0.12–0.15 fm^{-1}, it is related to the core bounce after which the central density and temperature decrease slightly before they continue to increase during the later compression. The wide stretched mixed phase region for the bag model in graph (a) results from the applied Gibbs construction while the in comparison narrow region for the PNJL model in graph (b) is a result of the Maxwell construction.

2. Total pressure density curves for different entropies per baryon and fixed $Y_p = 0.3$, based on the two hybrid EoS.

3. Radial profiles of velocity, density and temperature for a 15 $M_\odot$ progenitor model at selected post bounce times during the QCD phase transition induced PNS collapse, using the bag model with $B^{1/4} = 155$ MeV and $\alpha_S = 0.3$.

4. Evolution of the neutrino luminosities and mean energies for a 15 $M_\odot$ model, including the quark hadron phase transition using the quark bag model ($B^{1/4} = 155$ MeV, $\alpha_S = 0.3$) [40, 41]. Due to the phase transition, the PNS becomes gravitational unstable and collapses. The critical conditions for the gravitational collapse ($T = 17.67$ MeV, $\rho = 5.511 \times 10^{14}$ g/cm^3, $Y_p = 0.197$) are obtained at about 308 ms after bounce for this particular model. The second burst is released when the second shock, that forms due to the quark hadron phase transition in the PNS interior, crosses the neutrinospheres. The second burst occurs in all neutrino flavors, while the deleptonization burst at core bounce appears only in ν_e. This signature of deconfinement is absent in models that explore standard hadronic EoSs (e.g. from ref. [2]).